Thermodynamics and critical behavior in the Nambu–Jona-Lasinio model of QCD

P. Costa,[*] M. C. Ruivo,[+] and C. A. de Sousa[‡]

Departamento de Física, Universidade de Coimbra, P-3004-516 Coimbra, Portugal

(Received 27 July 2007; revised manuscript received 11 February 2008; published 19 May 2008)

We investigate the phase diagram of strongly interacting matter as a function of temperature and baryonic density/chemical potential, within Nambu–Jona-Lasinio type models. We perform a systematic study concerning the existence, location, and properties of a critical end point/tricritical point, both in SU (2) and SU(3) versions of the model. We verify that, for $m_u = m_d = 0$ and up to a critical strange quark mass, there is a tricritical point, which becomes a critical end point in a world with realistic values of the current quark masses. The properties of physical observables, such as the baryon number susceptibility and the specific heat, are analyzed in the vicinity of the critical end point, with special focus on their critical exponents. The behavior of mesons in the $T - \mu_B(\rho_B)$ plane is analyzed in connection with possible signatures of partial and effective restoration of chiral symmetry.

DOI: 10.1103/PhysRevD.77.096001 PACS numbers: 11.30.Rd, 11.55.Fv, 14.40.Aq

I. INTRODUCTION

Recently there has been encouraging progress on nonperturbative studies of the QCD thermodynamics which have stimulated a great deal of theoretical activity. Phenomenological and microscopic models have been developed along parallel and complementary lines allowing to predict a rich phase structure at finite temperature, T, and chemical potential, μ_B [1–4]. The quark gluon plasm (QGP) is a long-standing theoretical issue since the discovery of the asymptotic freedom of QCD [3,5]. Besides the intrinsic theoretical interest of this subject, such studies are important because they are directly applicable to the regime under current experimental investigation at the Brookhaven National Laboratory (BNL) Relativistic Heavy Ion Collider (RHIC). In fact, extensive experimental work has been done with heavy-ion collisions at CERN and Brookhaven to explore the $T - \mu_B$ phase diagram and look for signatures of the QGP.

Theoretical studies have been accumulating a lot of evidence that there exists a critical end point (CEP) in the phase diagram of strongly interacting matter. Since Fodor and Katz, who presented a phase diagram with the CEP within lattice calculations [6], remarkable progress in this area has been made. It is an open question whether a critical end point exists on the $T - \mu_B$ plane and, particularly, how to predict its location. When only thermal effects are concerned, universal arguments [7,8] and lattice simulations [9] indicate that the order of the phase transition depends on the masses and flavors of quarks.

Considering also nonvanishing chemical potentials, a variety of models (see e.g. [10,11]) predict a second order phase transition point in the phase diagram. This suggests that the phase diagram exhibits a CEP. At this point the phase transition is of second order and long wavelength fluctuations appear, leading to characteristic experimental consequences that can be detected by enhanced critical fluctuations in heavy-ion collisions [12,13]. So, the location of the CEP has become an important topic in effective model studies and lattice calculations. In fact, the phase diagram and QCD thermodynamics in general are becoming more transparent due to the combination of research in several areas: perturbative QCD, effective models, and lattice calculations.

The possible existence of such a point has recently been emphasized and its universal critical properties have been discussed by several authors in the context of QCD inspired models [10,11,14,15]. This point of the phase diagram is the special focus of the present article.

In a previous work [15], we studied the phase diagram focusing our attention on the CEP and the physics near it, through the behavior of the baryon number susceptibility and the specific heat; the study was performed in the framework of the SU(3) Nambu–Jona-Lasinio (NJL) model. Here, besides extending the investigation to other observables, we make a comparative study of the phase diagram in the SU(2) and SU(3) NJL models. Since more information can be taken within the simpler version of the NJL model, this systematic study is expected to provide a better understanding of the interesting physics around the CEP/tricritical point (TCP). Our main goal is to locate the critical end point and confront the results with universality arguments. Based on the fact that the CEP is a genuine thermodynamic singularity, being considered a second order critical point, the order parameter and related observables, like susceptibilities, can provide relevant signatures for phase transitions. We notice that susceptibilities in general are related to fluctuations through the fluctuation dissipation theorem, allowing to observe signals of phase transitions in heavy-ion reactions [16]. The specific heat C, which is related to the event-by-event temperature fluctuation [17], and mean transverse momentum fluctuations [18]

[*]pcosta@teor.fis.uc.pt
[+]maria@teor.fis.uc.pt
[‡]celia@teor.fis.uc.pt

in heavy-ion reactions, is also a quantity of interest in our calculation. These fluctuations should show a divergent behavior near the CEP. After equilibration, the dense matter created in relativistic heavy-ion collision will expand along lines of constant entropy per baryon.

We remark that most of the work done in this area has been performed with nonstrange quarks only and, when strange quarks are considered, mixing between the flavors u, d, and s has not been taken into account [19]. Our SU(3) version of the NJL model includes a term that incorporates the axial anomaly of QCD, and is responsible for the mechanism of flavor mixing. We relate the discontinuity of the order parameter to other discontinuities of physical quantities such as, for instance, the entropy. We are particularly interested in confronting our calculation, in what concerns to the notion of a second order phase transition due to nonvanishing current quark masses, with those of any classical mean field theory. From lattice calculations it is well known that the strange quark mass plays a decisive role in the location of the CEP.

On the other hand, information on the nature of excitations and the strength of their interaction in the QGP would be crucial in the experimental search. Also in this context it is relevant to confront first-principle based approaches with the results of phenomenological models like the NJL model.

We organize the work in four main steps. First, after the presentation of the model formalism (Sec. II), we discuss the behavior of the equations of state and analyze the chiral phase transition (Sec. III). The well-known universality hypothesis of phase transitions will be considered. Second, we study the behavior of relevant physical quantities in the $T-\mu_B$ plane (Sec. IV). Third, we analyze the phase diagrams in the $T-\mu_B$ plane looking for the location of the critical end point and the behavior of susceptibilities (Sec. V). Finally, we discuss signs of *partial* and *effective* restoration of chiral symmetry (Sec. VI), looking for the convergence of chiral partners. We conclude in Sec. VII with a brief summary of our results.

II. FORMULATION OF THE MODEL

The Lagrangian of the SU(3) NJL model [20–22] is given by

$$\mathcal{L} = \bar{q}(i\partial\cdot\gamma - \hat{m})q + \frac{g_S}{2}\sum_{a=0}^{8}[(\bar{q}\lambda^a q)^2 + (\bar{q}(i\gamma_5)\lambda^a q)^2] + g_D[\det[\bar{q}(1+\gamma_5)q] + \det[\bar{q}(1-\gamma_5)q]]. \quad (1)$$

The column vector $q = (u, d, s)$ represents the quark field with three flavors, $N_f = 3$, and three colors, $N_c = 3$. λ^a are the Gell-Mann matrices, a $= 0, 1, \ldots, 8$, $\lambda^0 = \sqrt{\frac{2}{3}}\mathbf{I}$.

The Lagrangian (1) is invariant under chiral $SU_L(3) \otimes SU_R(3)$ transformations if we put $m_i = 0$, where m_i are the current quark masses ($\hat{m} = \mathrm{diag}(m_u, m_d, m_s)$). The last term in (1) breaks the $U_A(1)$ symmetry. This term is a reflection of the axial anomaly in QCD.

The model Lagrangian (1) can be put in a form suitable for the bosonization procedure after an adequate treatment of the last term, allowing to obtain a four quark interaction from the six quark interaction. Then the following effective quark Lagrangian is obtained:

$$\mathcal{L}_{\mathrm{eff}} = \bar{q}(i\gamma^\mu\partial_\mu - \hat{m})q + S_{ab}[(\bar{q}\lambda^a q)(\bar{q}\lambda^b q)] + P_{ab}[(\bar{q}i\gamma_5\lambda^a q)(\bar{q}i\gamma_5\lambda^b q)], \quad (2)$$

where the projectors S_{ab}, P_{ab} are given by:

$$S_{ab} = g_S\delta_{ab} + g_D D_{abc}\langle\bar{q}\lambda^c q\rangle, \quad (3)$$

$$P_{ab} = g_S\delta_{ab} - g_D D_{abc}\langle\bar{q}\lambda^c q\rangle. \quad (4)$$

The constants D_{abc} coincide with the SU(3) structure constants d_{abc} for $a, b, c = (1, 2, \ldots, 8)$ and $D_{0ab} = -\frac{1}{\sqrt{6}}\delta_{ab}$, $D_{000} = \sqrt{\frac{2}{3}}$. The hadronization procedure can be done by the integration over the quark fields in the functional integral with (2). The natural degrees of freedom of low-energy QCD in the mesonic sector are achieved which gives the following effective action:

$$W_{\mathrm{eff}}[\varphi, \sigma] = -\tfrac{1}{2}(\sigma^a S^{-1}_{ab}\sigma^b) - \tfrac{1}{2}(\varphi^a P^{-1}_{ab}\varphi^b) - i\mathrm{Tr}\ \ln[i\gamma^\mu\partial_\mu - \hat{m} + \sigma_a\lambda^a + (i\gamma_5)\times(\varphi_a\lambda^a)]. \quad (5)$$

The notation Tr stands for the trace operation over discrete indices (N_f and N_c) and integration over momentum. The fields σ^a and φ^a are scalar and pseudoscalar meson nonets, respectively.

The first variation of the action (5) leads to the gap equations,

$$M_i = m_i - 2g_S\langle\bar{q}_i q_i\rangle - 2g_D\langle\bar{q}_j q_j\rangle\langle\bar{q}_k q_k\rangle, \quad (6)$$

with $i, j, k = u, d, s$ cyclic. M_i are the constituent quark masses and the quark condensates are given by: $\langle\bar{q}_i q_i\rangle = -i\mathrm{Tr}[S_i(p)]$, $S_i(p)$ being the quark Green function.

The baryonic thermodynamic potential of the grand canonical ensemble, $\Omega(T, V, \mu_i)$, is also obtained directly from the effective action (5). So we take the temperature T, the volume V, and the chemical potential of the i-quark (μ_i) as the full independent state variables.

The relevant equations of state for the entropy S, the pressure p, and the particle number N_i, as well as the internal energy E, follow from well-known expressions like the Gibbs-Duhem relation

$$\Omega(T, V, \mu_i) = E - TS - \sum_{i=u,d,s}\mu_i N_i. \quad (7)$$

The following expressions are obtained:

$$E = -\frac{N_c}{\pi^2} V \sum_{i=u,d,s} \left\{ \int p^2 dp \frac{p^2 + m_i M_i}{E_i} (1 - n_i - \bar{n}_i) \right\} - g_S \sum_{i=u,d,s} (\langle \bar{q}_i q_i \rangle)^2 - 2 g_D \langle \bar{u}u \rangle \langle \bar{d}d \rangle \langle \bar{s}s \rangle, \quad (8)$$

$$S = -\frac{N_c}{\pi^2} V \sum_{i=u,d,s} \int p^2 dp \{ [n_i \ln n_i + (1 - n_i) \ln(1 - n_i)] + [n_i \to 1 - \bar{n}_i] \}, \quad (9)$$

$$N_i = \frac{N_c}{\pi^2} V \int p^2 dp (n_i - \bar{n}_i). \quad (10)$$

V is the volume of the system and the quark density is determined by the relation $\rho_i = N_i/V$. In the previous equations n_i and $\bar{n}_i$ are the quark and antiquark occupation numbers

$$n_i = \frac{1}{1 + e^{\beta(E_i - \mu_i)}}, \qquad \bar{n}_i = \frac{1}{1 + e^{\beta(E_i + \mu_i)}}. \quad (11)$$

We define $\mu_B = \frac{1}{3}(\mu_u + \mu_d + \mu_s)$ and the baryonic matter density as $\rho_B = \frac{1}{3}(\rho_u + \rho_d + \rho_s)$. As usual, the pressure and the energy density are defined such that their values are zero in the vacuum state [23]:

$$p(\mu_i, T) = -\frac{1}{V}[\Omega(\mu_i, T) - \Omega(0, 0)], \quad (12)$$

$$\epsilon(\mu_i, T) = \frac{1}{V}[E(\mu_i, T) - E(0, 0)]. \quad (13)$$

The baryon number susceptibility is the response of the baryon number density $\rho_B(T, \mu_i)$ to an infinitesimal variation of the quark chemical potential μ_i [24]:

$$\chi_B = \frac{1}{3} \sum_{i=u,d,s} \left(\frac{\partial \rho_i}{\partial \mu_i} \right)_T. \quad (14)$$

Another relevant observable, in the context of possible signatures in chiral symmetry restoration in the hadron-quark transition and for transition from hadronic matter to the QGP [24–26], is the specific heat which is defined by [15]

$$C = \frac{T}{V} \left(\frac{\partial S}{\partial T} \right)_{N_i} = \frac{T}{V} \left[\left(\frac{\partial S}{\partial T} \right)_{\mu_i} - \frac{[(\partial N_i/\partial T)_{\mu_i}]^2}{(\partial N_i/\partial \mu_i)_T} \right], \quad (15)$$

where we have transformed the derivative $(\partial S/\partial T)_{N_i}$ using the formula of the Jacobian. In fact, we work in the grand canonical ensemble where (T, V, μ_i) are the set of natural independent variables (still holding N_i and V fixed).

By expanding the effective action (5) over meson fields, we get an effective meson action from which we can obtain the meson propagators. In the present work we are only concerned with π^0 and σ mesons. Starting with the pseudoscalar mesons we have the effective meson action:

$$W^{(2)}_{\text{eff}}[\varphi] = -\tfrac{1}{2}\varphi^a [P^{-1}_{ab} - \Pi^P_{ab}(P)]\varphi^b = -\tfrac{1}{2}\varphi^a (D^P_{ab}(P))^{-1}\varphi^b, \quad (16)$$

where $\Pi^P_{ab}(P)$ is the polarization operator,

$$\Pi^P_{ab}(P) = iN_c \int \frac{d^4 p}{(2\pi)^4} \text{tr}_D [S_i(p)(\lambda^a)_{ij}(i\gamma_5) S_j(p + P) \times (\lambda^b)_{ji}(i\gamma_5)], \quad (17)$$

with tr_D is the trace over Dirac matrices. The expression in square brackets in (16) is the inverse non-normalized meson propagator $(D^P_{ab}(P))^{-1}$.

The inverse meson propagator for π^0 is given by

$$D^{-1}_{\pi^0}(P) = 1 - P_{\pi^0} J^P_{uu}(P), \quad (18)$$

with

$$P_{\pi^0} = g_S + g_D \langle \bar{q}_s q_s \rangle \quad (19)$$

and where the polarization operator of the π^0 meson takes the form

$$J^P_{uu}(P_0) = 4[2I^u_1 - P^2_0 I^{uu}_2(P_0)]. \quad (20)$$

The integrals I^i_1 and $I^{ij}_2(P_0)$ are given in Appendix A.

The mass of the π^0 meson can be determined by the condition $D^{-1}_{\pi^0}(M_{\pi^0}, \mathbf{0}) = 0$ and the quark-meson coupling constant is evaluated as

$$g^{-2}_{\pi^0 \bar{q}q} = -\frac{1}{2M_{\pi^0}} \frac{\partial}{\partial P_0} [J^P_{uu}(P_0)]_{|_{P_0 = M_{\pi^0}}}. \quad (21)$$

The procedure to describe scalar mesons is analogous. We present below the most relevant steps. Keeping now the scalar mesons only in (5), we have the effective meson action

$$W^{(2)}_{\text{eff}}[\sigma] = -\tfrac{1}{2}\sigma^a [S^{-1}_{ab} - \Pi^S_{ab}(P)]\sigma^b = -\tfrac{1}{2}\sigma^a (D^S_{ab}(P))^{-1}\sigma^b, \quad (22)$$

with $\Pi^S_{ab}(P)$ being the polarization operator, which in the momentum space has the form of (17) with $(i\gamma_5)$ substituted by the identity matrix.

To consider the σ meson we take into account the matrix structure of the propagator in (22). For the isospin symmetry considered in the present work $\langle \bar{q}_u q_u \rangle = \langle \bar{q}_d q_d \rangle$, and the matrices S_{ab} and Π^S_{ab} are reduced to

$$S_{ab} \to \begin{pmatrix} S_{33} & 0 \\ 0 & \bar{S}_{ab} \end{pmatrix} \quad \text{and} \quad \Pi^S_{ab} \to \begin{pmatrix} \Pi^S_{33} & 0 \\ 0 & \bar{\Pi}^S_{ab} \end{pmatrix}, \quad (23)$$

where the matrix elements are given in Appendix A.

The mass of the σ meson can be determined by the condition $D^{-1}_{\sigma}(M_{\sigma}, \mathbf{0}) = 0$, where

$$D^{-1}_{\sigma} = (\mathcal{A} + \mathcal{C}) - \sqrt{(\mathcal{C} - \mathcal{A})^2 + 4\mathcal{B}^2} \quad (24)$$

with $\mathcal{A} = S_{88} - \Delta\Pi^S_{00}(P)$, $\mathcal{C} = S_{00} - \Delta\Pi^S_{88}(P)$, $\mathcal{B} = -(S_{08} + \Delta\Pi^S_{08}(P))$, and $\Delta = S_{00}S_{88} - (S_{08})^2$.

Finally, the model is fixed by the coupling constants g_S and g_D, the cutoff in three-momentum space Λ, which is used to regularize the momentum space integrals and the current quark masses m_i. For numerical calculations in physical conditions we use the parameter set [22,27–29]: $m_u = m_d = 5.5$ MeV, $m_s = 140.7$ MeV, $g_S\Lambda^2 = 3.67$, $g_D\Lambda^5 = -12.36$, and $\Lambda = 602.3$ MeV, that has been determined by fixing the values $M_\pi = 135.0$ MeV, $M_K = 497.7$ MeV, $f_\pi = 92.4$ MeV, and $M_{\eta'} = 960.8$ MeV. For the quark condensates we obtain: $\langle\bar{q}_u q_u\rangle = \langle\bar{q}_d q_d\rangle = -(241.9\ \text{MeV})^3$ and $\langle\bar{q}_s q_s\rangle = -(257.7\ \text{MeV})^3$, and for the constituent quark masses $M_u = M_d = 367.7$ MeV and $M_s = 549.5$ MeV.

III. EQUATIONS OF STATE AND PHASE TRANSITION

We will start the discussion of the phase diagram of the NJL model (1) by analyzing the behavior of the pressure/energy per particle as a function of the baryonic density, paying special attention to the Gibbs criteria. Our model of strong interacting matter can simulate either a region in the interior of a neutron star or a hot and dense fireball created in a heavy-ion collision. In the present work we focus our attention in the last type of systems, so we impose the condition $\mu_e = 0$, since electrons and positrons are not involved in the strong interaction. So, we naturally get the chemical equilibrium condition $\mu_u = \mu_d = \mu_s = \mu_B$ that will be used. This choice allows for equal constituent quark masses $M_u = M_d$ and approximates the physical conditions at RHIC. In this respect, we remind that in a relativistic heavy-ion collision of duration of $\sim 10^{-22} s$, thermal equilibration is possible only for processes mediated by the strong interaction rather than the full electroweak equilibrium.

Let us discuss our results for the pressure/energy per baryon at zero temperature that are plotted in Fig. 1 as a function of ρ_B/ρ_0 (solid lines), where $\rho_0 = 0.17$ fm^{-3} is the normal nuclear matter density. The pressure has three zeros, respectively, at $\rho_B = 0, 0.43\rho_0, 2.36\rho_0$, that correspond to the extreme of the energy per particle. For $\rho_B < 0.2\rho_0$ the pressure and compressibility are positive, so the system can exist in a uniform gas phase, but it will not survive indefinitely, since the zero density state is energetically favored; for $0.2\rho_0 < \rho_B < 0.43\rho_0$ the system is unstable since the compressibility is negative, in fact $\rho_B = 0.43\rho_0$ corresponds to a maximum of the energy per particle; for $0.43\rho_0 < \rho_B < 2.36\rho_0$, the pressure is negative, and the third zero of the pressure, $\rho_B = 2.36\rho_0$, corresponds to an absolute minimum of the energy [see Fig. 1 (right panel)]. The appearance of an absolute minimum of the energy means the possibility for finite droplets to be in mechanical equilibrium with the vacuum at zero pressure ($P = 0$). Above $\rho_B = 2.36\rho_0$, which we define as ρ_B^{cr}, we have again a uniform gas phase. So, for densities $0 < \rho_B < \rho_B^{\text{cr}}$ the equilibrium configuration is a mixed phase. This is because the Gibbs criterion of equal P and μ_B is satisfied and, therefore, the phase transition is a first order one: the thermodynamic potential has two degenerate minima at which two phases have equal pressure and chemical potential and can coexist. Such a situation is possible in regions where the gap equations have several solutions for the quark masses.

Summarizing the results at $T = 0$, the behavior described allows the following interpretation: the uniform nonzero density phase will break up into stable droplets with zero pressure and density $\rho_B^{\text{cr}} = 2.36\rho_0$ in which chiral symmetry is partially restored, surrounded by a nontrivial vacuum with $\rho_B = P = 0$ (see also [10,23,27,30,31]). In fact, for our choice of the parameters the critical point at $T = 0$ satisfies to the condition $\mu_i < M_i^{\text{vac}}$ [23,32], where M_i^{vac} is the mass of the i-quark in the vacuum. This can be seen by comparing $\mu_B^{\text{cr}} = 361$ MeV (see the T-axis of Fig. 2, left panel) with the quark masses $M_u^{\text{vac}} = M_d^{\text{vac}} = 367.7$ MeV and $M_s^{\text{vac}} = 549.5$ MeV.

As can be seen from Fig. 1, as the temperature increases, the first order transition persists up to the CEP. At the CEP the chiral transition becomes of second order. Along the

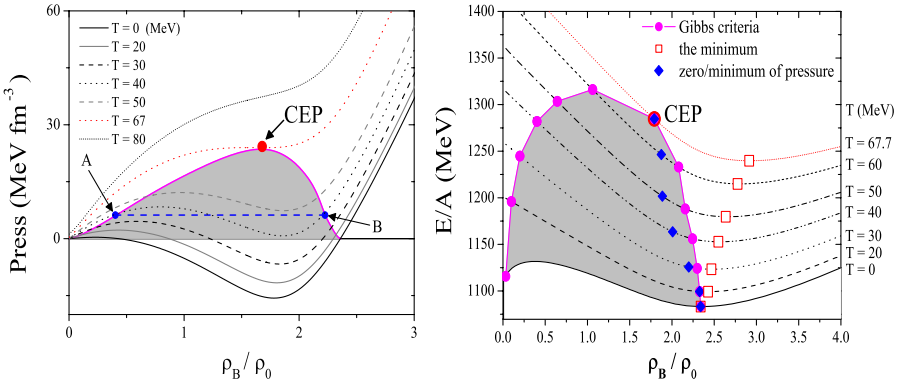

FIG. 1 (color online). Pressure (left) and energy per particle (right) as a function of the density at different temperatures. The points A and B (left panel) illustrate the Gibbs criteria. Only in the $T = 0$ line the zero-pressure point is located at the minimum of the energy per particle.

line of a first order phase transition the thermodynamic potential has two degenerate minima. These minima are separated by a finite potential barrier making the potential nonconvex. The height of the barrier is largest at zero temperature and finite quark chemical potential and decreases towards higher temperature. At the CEP the barrier disappears and the potential flattens. This pattern is characteristic of a first order phase transition: the two minima correspond, respectively, to the phases of broken and restored symmetry. The borders of the coexistence area are marked by the dotted lines in Fig. 2. The domain between the two dotted lines has metastable states which are characterized by large fluctuations. They are also solutions of the gap equations but their thermodynamic potential is higher than for the stable solutions. The left dotted curves represent the beginning of the metastable solutions of restored symmetry in the phase of broken symmetry, while the right dotted curves represent the end of the metastable solutions of broken symmetry in the restored symmetric phase. We also represent in Fig. 2 (right panel) the region where the solutions of the gap equations are unstable.

The location of the CEP is found to be at $T^{\mathrm{CEP}} = 67.7$ MeV and $\rho_B^{\mathrm{CEP}} = 1.68\rho_0$ ($\mu_B^{\mathrm{CEP}} = 318.4$ MeV). For temperatures above the CEP the thermodynamic potential has only one minimum and the transition is washed out: a smooth crossover takes place.

Finally, we will focus again on the energy per baryon. In Fig. 1 (right panel), we plot the density dependence of the energy per baryon at different temperatures. We observe that the two points, zero of the pressure and minimum of the energy density, are not the same at finite temperature. In fact, as can be seen from Fig. 1 (left panel), states with zero pressure are only possible up to the maximal temperature $T_m \sim 38$ MeV. We notice that the zero-pressure states persist up to temperatures of 70 MeV in a two-flavor NJL model where equal chemical potentials of quarks and antiquarks is assumed [30]. For $T < T_m$ the zero-pressure states are in the metastable density region and, as soon as $T \neq 0$, they do not coincide with the minimum of the energy per particle.

The arguments just presented allow to clarify the difference between confined quark matter (in hadrons) and bounded quark matter (droplets of quarks). As would be expected, the binding mechanism is weaker than the confining one (nonexistent in the NJL model). As a matter of fact, in spite of the existence of a binding energy for the droplets of quarks at $T = 0$, we verify that it is not possible to avoid the evaporation of the bounded quarks for arbitrarily small temperatures.

More detailed information concerning the structure of the phase diagram will be given in Sec. V.

IV. THERMODYNAMIC QUANTITIES IN THE $T - \mu_B$ PLANE

For a better understanding of the thermodynamics of the phase transitions, we analyze in this section the behavior of the thermodynamical quantities that are the most relevant to discuss the physics across the first order phase transition. With these quantities, we can also discuss the latent heat which is inherent to this phase transition.

The pressure is plotted in the left-hand side of Fig. 3 (upper part), which shows a continuous behavior for all points of the phase diagram. In a first order phase transition a discontinuity occurs in the first derivatives of the pressure (or the thermodynamic potential) with respect to μ_B and T, i.e., the baryon number density and the entropy density, respectively. In fact, as can be seen in the right side of Fig. 3, the entropy density is discontinuous in the first order phase transition region ($T < T^{\mathrm{CEP}}$, $\mu_B > \mu_B^{\mathrm{CEP}}$). A similar behavior is found for the energy density, which curves show that the first order phase transition, strong at $T = 0$, turns into a less abrupt one as the temperature increases (see Fig. 3, lower part). In the crossover transition ($T > T^{\mathrm{CEP}}$, $\mu_B < \mu_B^{\mathrm{CEP}}$) the thermodynamic quantities change rapidly within a narrow range of values of T and μ_B, but

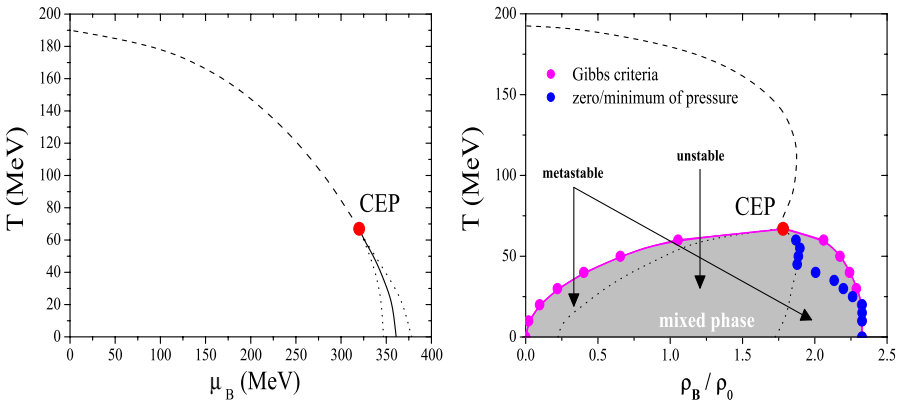

FIG. 2 (color online). Phase diagram in the SU(3) NJL model. The left (right) part corresponds to the $T - \mu_B$ ($T - \rho_B$) plane. Solid (dashed) line shows the location of the first order (crossover) transition. The dotted lines show the location of the spinodal boundaries of the two phase transitions (shown by shading in the right plot).

the pressure and all its derivatives remain continuous, as shown in Fig. 3.

The discontinuities of the entropy and energy densities disappear at the CEP, whose location cannot be determined by universality arguments. The same is not true concerning local singular behavior of thermodynamic quantities around the CEP that will be discussed in the next section through the critical exponents.

Let us now analyze what information concerning the latent heat we can get from our results. As already referred to in Sec. III, along the line of first order phase transition the thermodynamic potential has two degenerate minima that are separated by a finite barrier. This barrier is largest at zero temperature and finite chemical potential and decreases towards higher temperature. At the CEP the barrier disappears, which means that there is no latent heat at this point.

As a grand canonical approach is applied to our model of strong interacting matter, the independent quantities T and μ_B represent the state variables which can be externally controlled. So, the conjugate of the intensive variables T and μ_B in the Legendre transformation—the entropy density s and the baryonic density ρ_B—provide a more natural description. By analyzing first the gap in the curves of the entropy (Fig. 3, right side of upper part), we see that the latent heat decreases for small temperatures, which is not the expected behavior. This analysis is, however, not sufficient; both the baryonic density and the entropy density contributions should be examined for more reliable information about the latent heat. We remember that the gap of the baryonic density across the first order phase transition is largest at zero temperature and finite chemical potential and vanishes at the CEP (see Fig. 2, right panel). The discontinuities in the energy density include both the entropy and the baryonic density contributions and, as can be seen in Fig. 3, they display the expected behavior: the latent heat increases for decreasing temperatures.

Finally, to understand the thermodynamics of matter created in relativistic heavy-ion collisions, it is convenient to calculate thermodynamic quantities along lines of constant entropy per baryon number, the so-called isentropic lines. Most of these studies have been done on lattice calculations for two-flavor QCD at finite μ_B [33], where nonphysical mass spectrum that corresponds to a too large value of pion mass $m_\pi \simeq 770$ MeV, has been used. Such studies predict that the effects of the CEP change only slowly as the collision energy is changed as a consequence of the attractor character of the CEP [12].

Our model calculations for the isentropic lines in the $T - \mu_B$ plane are shown in Fig. 4. The behavior we find is somewhat different from those claimed by other authors [33–35], where a phenomena of focusing of trajectories towards the CEP is observed.

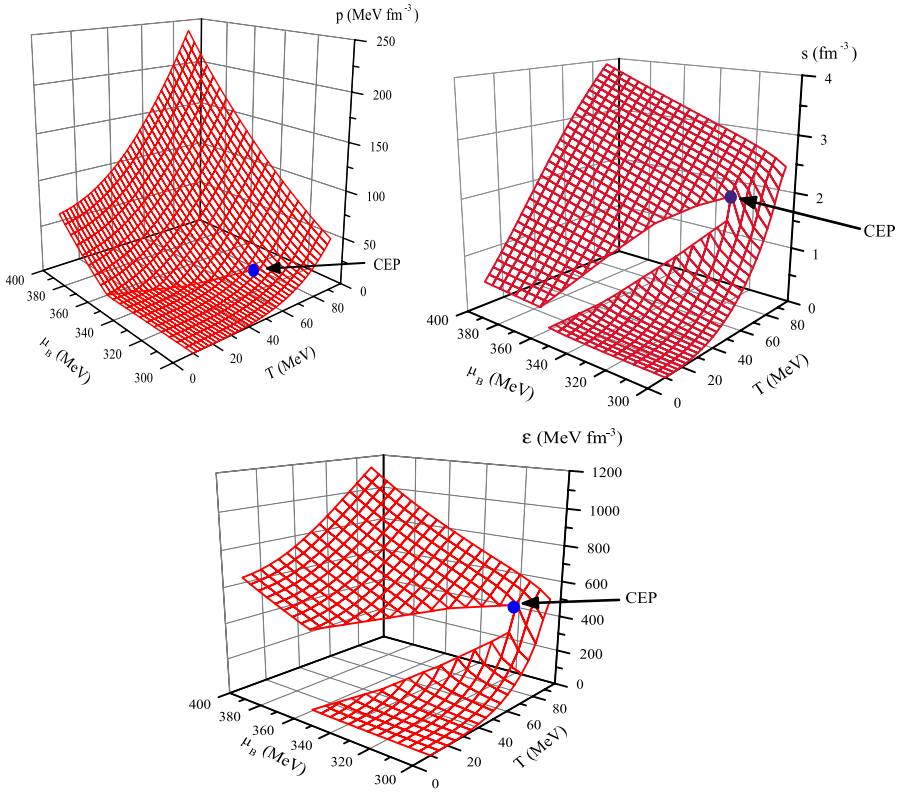

FIG. 3 (color online). Pressure (left side of upper part), entropy density (right side of upper part), and energy density (down part) as functions of the temperature and the baryonic chemical potential.

The isentropic trajectories in the phase diagram (Fig. 4) indicate that the slope of the trajectories goes to large values for large T. This behavior is related to the effects of the strange quark mass in our model. In fact, at high temperatures the relation $\mu_s > M_s$ is verified, allowing for a more pronounced decrease of M_s [27]. Although the entropy and the baryon number density, at high temperatures, are sensitive to the regularization procedure used [36,37], this effect is not relevant for the present situation. The same is not true with respect to the effects of the value of the cutoff itself in the regime of low temperatures as will be shown below.

In a small range of s/ρ_B around 0.7 (see Fig. 4, right panel), we observe a tendency of convergence of these isentropic lines towards the CEP. These lines come from the region of symmetry partially restored in the direction of the crossover line. For smaller values of s/ρ_B, the isentropic lines turn about the CEP and then attain the first order transition line. For larger values of s/ρ_B the isentropic trajectories approach the CEP by the region where the chiral symmetry is still broken, and also attain the first order transition line after bending toward the critical point. As already pointed out in [32], this is a natural result in these type of quark models with no change in the number of degrees of freedom of the system in the two phases. As the temperature decreases a first order phase transition occurs, the latent heat increases, and the formation of the mixed phase is thermodynamically favored.

Finally, we remark that all isentropic trajectories directly terminate at $T = 0$ at the first order transition line, without reheating in the mixed phase as verified in the "zigzag" shape of [33–35,38]. It is also interesting to point out that, in the limit $T \to 0$, it is verified that $s \to 0$ and $\rho_B \to 0$, as it should be. This behavior is in contrast to [32] (right panel Fig. 9) using the NJL model in the SU(2) sector and is related to our more convenient choice of the model parameters, mainly a lower value of the cutoff. This can be explained by the presence of droplets at $T = 0$ whose stability is quite sensitive to the choice of the model parameters. In fact, as referred to in Sec. III, our choice of the parameters has important effects: we verify that, at $T = 0$, the phase transition connects the vacuum state ($P = 0$, $\rho_B = 0$) directly with the phase of chiral symmetry partially restored ($P = 0$, $\rho = \rho_B^{\rm cr}$) and the critical point of the phase transition in these conditions satisfies to $\mu_i < M_i^{\rm vac}$, where $M_i^{\rm vac}$ is the mass of the i-quark ($i = u, d, s$) in the vacuum. This condition fulfills the criterium of stability of the quark droplets [23,27]. In addition, it is also crucial to the satisfaction of the third law of thermodynamics in the limit $T \to 0$. This cutoff effect has an identical role in the formation of stable droplets on both SU(2) and SU(3) NJL models.

V. PHASE DIAGRAMS AND SUSCEPTIBILITIES IN THE VICINITY OF THE CRITICAL END POINT

In this section we analyze with more detail the phase diagrams in different conditions in the $T - \mu_B$ plane. Lattice QCD calculations have established the transition to a phase where quarks and gluons are deconfined at temperatures larger than $\sim$150 MeV and zero baryon density. Depending on the number of quark flavors $N_f = 2$ or $N_f = 3$, and on the masses of the quarks, different situations can occur and the transition from hadronic matter to QGP may be of first order, second order, or a crossover transition. To confront the model results with the universality arguments, we will discuss the class of the critical points by changing the current quark masses in SU(2) and SU(3) versions of the NJL model.

A. Characteristics of the $T - \mu_B$ phase diagram

We start by analyzing the differences between the three-flavor NJL model and its simpler version in the SU(2) sector. The phase diagrams for both models are presented in Fig. 5 as a function of μ_B and T.

Concerning the SU(2) model, and using physical values of the quark masses: $m_u = m_d = 5.5$ MeV, we find that

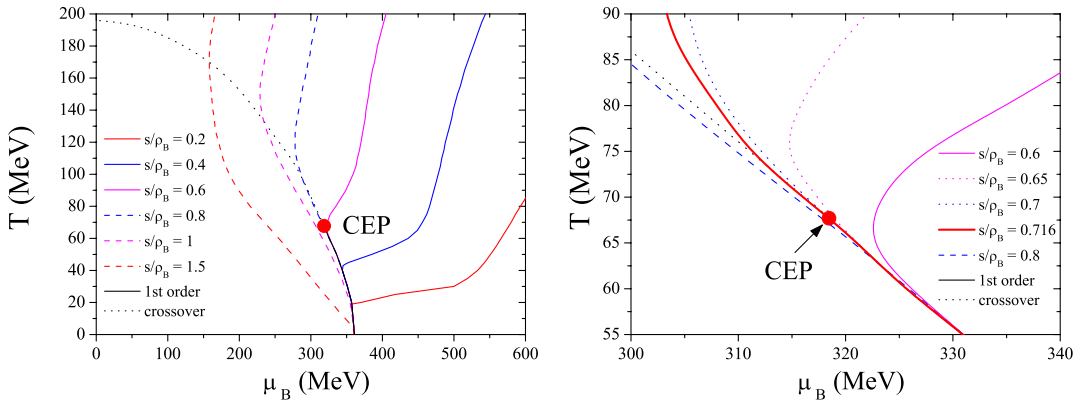

FIG. 4 (color online). Two perspectives of the entropy per baryon number in the $T - \mu_B$ plane. The vicinity of the CEP is enlarged in the right panel.

the CEP is localized at $T^{\mathrm{CEP}} = 79.9$ MeV and $\mu_B^{\mathrm{CEP}} = 331.72$ MeV ($\rho_B^{\mathrm{CEP}} = 2.26\rho_0$). We also verified that, in the chiral limit, the transition is of second order at $\mu_B = 0$ and, as μ_B increases, the line of second order phase transition will end in a first order line at the TCP. The TCP is located at $\mu_B^{\mathrm{TCP}} = 286.1$ MeV and $T^{\mathrm{TCP}} = 112.1$ MeV.

For the SU(3) NJL model, also in the chiral limit ($m_u = m_d = m_s = 0$), we verify that the phase diagram does not exhibit a TCP: chiral symmetry is restored via a first order transition for all baryonic chemical potentials and temperatures (see right panel of Fig. 5). According to lattice analysis, this pattern of chiral symmetry restoration should remain even when the strange quark acquires a nonzero current mass, provided it is lower than a critical value ($m_s < m_s^{\mathrm{crit}}$), and $m_u = m_d = 0$ is still kept. The value for m_s^{crit} is not settled yet, those found in lattice [39] or in model calculations [40,41] being lower than the physical strange current quark mass ($m_s \approx 150$ MeV). We found $m_s^{\mathrm{crit}} = 18.3$ MeV in our model [15], lower than lattice values [39] but consistent with what it is expected in these type of models [41].

When $m_s \geq m_s^{\mathrm{crit}}$, at $\mu_B = 0$, the transition is of second order and, as μ_B increases, the line of the second order phase transition will end in a first order line at the TCP. The TCP for $m_s = 140.7$ MeV is the closest to the CEP [15] and is located at $\mu_B^{\mathrm{TCP}} = 265.9$ MeV and $T^{\mathrm{TCP}} = 100.5$ MeV. If we choose $m_u = m_d \neq 0$, instead of second order transition we have a smooth crossover whose critical line will end in the first order line at the CEP. Using physical values for the quark masses [22,28]: $m_u = m_d = 5.5$ MeV, $m_s = 140.7$ MeV, this point is localized at $T^{\mathrm{CEP}} = 67.7$ MeV and $\mu_B^{\mathrm{CEP}} = 318.4$ MeV ($\rho_B^{\mathrm{CEP}} = 1.68\rho_0$).

We point out that both situations are in agreement with what is expected at $\mu_B = 0$: the chiral phase transition at the chiral limit is of second order for $N_f = 2$ and first order for $N_f \geq 3$ [42].

We also observe that the critical region is heavily stretched in the direction of the crossover transition line, in both $N_f = 2$ and $N_f = 3$ cases, as shown in Fig. 5. To estimate the critical region around the CEP we calculate the dimensionless ratio $\chi_B/\chi_B^{\mathrm{free}}$, where χ_B^{free} is the chiral susceptibility of a free massless quark gas. The left (right) panel of Fig. 5 shows a contour plot for two fixed ratios $\chi_B/\chi_B^{\mathrm{free}} = 2.0; 3.0$ in the phase diagram around the CEP.

B. Behavior of χ_B and C in the vicinity of the critical end point and their critical exponents

The phenomenological relevance of fluctuations in the finite temperature and chemical potential around the CEP/TCP of QCD has been recognized by several authors. If the critical region of the CEP is small, it is expected that most of the fluctuations associated with the CEP will come from the mean field region around the CEP [13]. The size of the critical region around the CEP can be found by calculating the baryon number susceptibility, the specific heat, and their critical behaviors.

To a better understanding of the critical behavior of the system, we also analyze in some detail what happens in the SU(2) case sector to which there is more information in the literature [43].

As is well known, the baryon number susceptibility χ_B and the specific heat C diverge at $T = T^{\mathrm{CEP}}$ [13,15,44]. In order to make this statement more precise, we will focus on the values of a set of indices, the so-called critical exponents, which describe the behavior near the critical point of various quantities of interest (in our case ϵ and α are the critical exponents of χ_B and C, respectively). The motivation for this study arises from fundamental phase transition considerations, and thus transcends any particular system. These critical exponents will be determined by finding two directions, temperature and magnetic-field-like, in the $T - \mu_B$ plane near the CEP, because, as pointed out in [45], the strength of the divergence is governed by the critical exponents whose values depend on the path approaching the CEP.

Considering the baryon number susceptibility, if the path chosen is asymptotically parallel to the first order transition

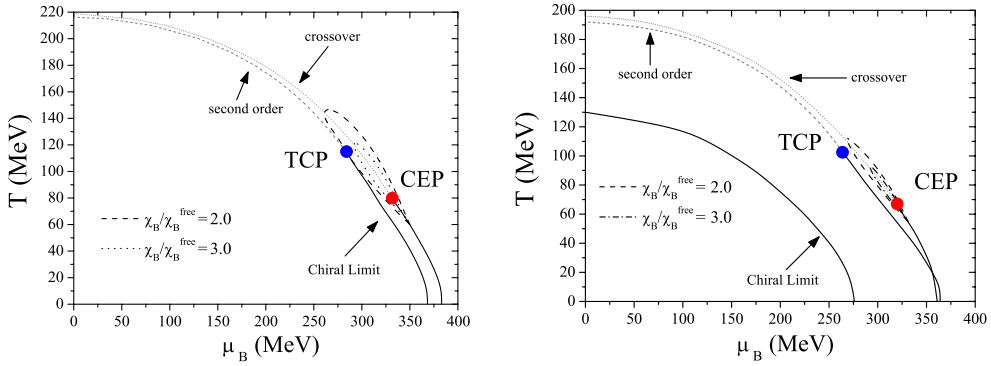

FIG. 5 (color online). Phase diagram in the SU(2) (left) and SU(3) (right) NJL models. The solid line represents the first order phase transition, the dashed line the second order phase transition, and the dotted line the crossover transition. The size of the critical region is also plotted for several values of $\chi_B/\chi_B^{\mathrm{free}}$. The TCP in the right panel is found for $m_u = m_d = 0$ MeV and $m_s = 140.7$ MeV.

line at the CEP, the divergence of χ_B scales with an exponent γ_B. In the mean field approximation it is expected that $\gamma_B = 1$ for this path. For directions not parallel to the tangent line the divergence scales as $\epsilon = 2/3$. These values are responsible for the elongation of the critical region, χ_B, being enhanced in the direction parallel to the first order transition line (see Fig. 5).

To study the critical exponents for the baryon number susceptibility (Eq. (14)) we will start with a path parallel to the μ_B-axis in the $T - \mu_B$ plane, from lower μ_B towards the critical $\mu_B^{\rm CEP}$, at fixed temperature $T = T^{\rm CEP}$. Using a linear logarithmic fit

$$\ln\chi_B = -\epsilon \ln|\mu_B - \mu_B^{\rm CEP}| + c_1, \tag{25}$$

where the term c_1 is independent of μ_B, we obtain $\epsilon = 0.67 \pm 0.01$, which is consistent with the mean field theory prediction $\epsilon = 2/3$.

We also study the baryon number susceptibility from higher μ_B towards the critical $\mu_B^{\rm CEP}$. The logarithmic fit used now is $\ln\chi_B = -\epsilon' \ln|\mu_B - \mu_B^{\rm CEP}| + c_1'$. Our result shows that $\epsilon' = 0.68 \pm 0.01$ which is very near the value of ϵ. This means that the size of the region we observe is approximately the same independently of the direction we choose for the path parallel to the μ_B-axis. These critical exponents, calculated in both SU(2) and SU(3) NJL models, are presented in Table I.

For comparison purposes with the universality/mean field predictions, the calculated critical exponents at the TCP are also presented in Table I. It is found that the critical exponent for χ_B, γ_B once we are in the TCP, has the value $\gamma_B = 0.49 \pm 0.02$, for the SU(3) NJL model and $\gamma_B = 0.51 \pm 0.01$, for the SU(2) NJL model. These results are in agreement with the mean field value ($\gamma_B = 1/2$), and show that the behavior of the baryon number susceptibility is similar in both SU(2) and SU(3) versions of the model.

Paying now attention to the specific heat (Eq. (15)) around the CEP, we have used a path parallel to the T-axis in the $T - \mu_B$ plane from lower/higher T towards the critical $T^{\rm CEP}$ at fixed $\mu_B = \mu_B^{\rm CEP}$. In Fig. 6 (upper part) we plot C as a function of T close to the CEP in a logarithmic scale for both SU(2) and SU(3) calculations. In this case we use the linear logarithmic fit $\ln C = -\alpha \ln|T - T^{\rm CEP}| + c_2$, where the term c_2 is independent of T. Starting with the SU(2) case, we observe in the left panel that, for the region $T < T^{\rm CEP}$, we have a slope of data points that changes for values of $|T - T^{\rm CEP}|$ around 0.3 MeV. We have fitted the data for $|T - T^{\rm CEP}| < 0.3$ MeV and $|T - T^{\rm CEP}| > 0.3$ MeV separately and obtained, respectively, the critical exponents $\alpha = 0.59 \pm 0.01$ and $\alpha_1 = 0.45 \pm 0.01$, which have a linear behavior for several orders of magnitude (see also Table I). As pointed out in [13], this change of the exponent can be interpreted as a crossover of different universality classes, with the CEP being affected by the TCP. It seems that in our model the effect of the hidden TCP on the CEP is relevant for the specific heat contrarily to what happens to χ_B.

We also observe that there is no clear evidence of the change of the slope of the fitting of data points in the three-flavor NJL model (see Fig. 6, right panel of upper part, and Table I). In fact, now we only obtain a critical exponent $\alpha = 0.61 \pm 0.01$ when the critical point is approached from below. When the critical point is approached from above the trivial exponent, $\alpha' = 0.67 \pm 0.01$ is obtained.

To explore the possible effect of the hidden TCP on the CEP, as suggested in Refs. [13,44], we analyze the behavior of the specific heat around the TCP. As shown in Fig. 6 (lower part) and Table I, we find nontrivial critical exponents $\alpha = 0.40 \pm 0.01$ and $\alpha = 0.45 \pm 0.01$, for SU(2) and SU(3) cases, respectively. This result, in spite of being close, is not in agreement with the respective mean field value ($\alpha = 1/2$). However, they can justify the crossing effect observed. We notice that the closest distance between the TCP and the CEP in the phase diagram occurs in the T-direction ($(T^{\rm TCP} - T^{\rm CEP}) < (\mu_B^{\rm CEP} - \mu_B^{\rm TCP})$).

TABLE I. The arrow $\rightarrow\cdot\binom{\cdot}{\uparrow}$ indicates the path in the $\mu_B(T)$-direction to the CEP (TCP) for $\mu_B < \mu_B^{\rm CEP}(T < T^{\rm TCP})$.

Quantity	Critical exponents/path	SU(2) NJL	SU(3) NJL	Universality
χ_B	ϵ / $\rightarrow$●	0.66 ± 0.01	0.67 ± 0.01	2/3
	ϵ' / ●$\leftarrow$	0.66 ± 0.01	0.68 ± 0.01	2/3
	γ_B / $\rightarrow$●	0.51 ± 0.01	0.49 ± 0.02	1/2
C	● / α	$\alpha = 0.59 \pm 0.01$	0.61 ± 0.01	2/3
	$\uparrow$	$\alpha_1 = 0.45 \pm 0.01$	—	—
	$\downarrow$ / α'	0.69 ± 0.01	0.67 ± 0.01	2/3
	●● / α	0.40 ± 0.01	0.45 ± 0.02	1/2
	$\uparrow$			

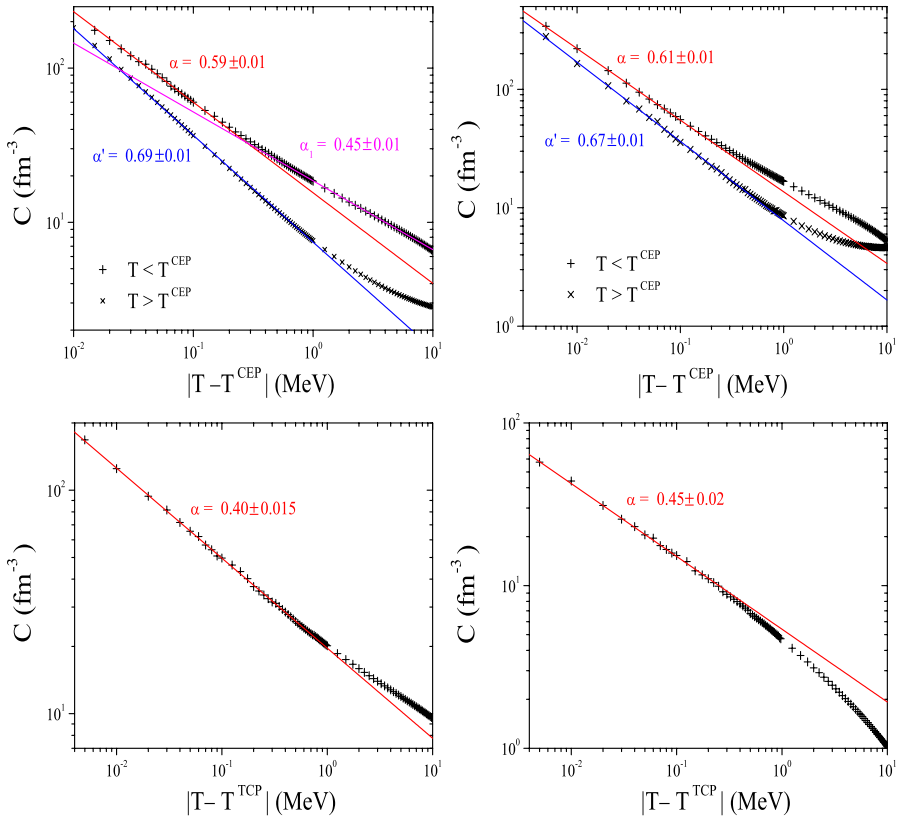

FIG. 6 (color online). Upper part: Specific heat as a function of $|T - T^{\mathrm{CEP}}|$ at the fixed chemical potential μ_B^{CEP} for SU(2) (left) and SU(3) (right) NJL models. Lower part: Specific heat as a function of $|T - T^{\mathrm{TCP}}|$ at the fixed chemical potential μ_B^{TCP} for SU(2) (left) and SU(3) (right) NJL models.

The inconsistency with the mean field values only occurs for the exponent α as can be seen from Table I. According to what was suggested by universality arguments in [13], it was expected that χ_B and C should be essentially the same near the TCP and the CEP, which would imply $\alpha = \epsilon = 2/3$ at the CEP. Nevertheless we observe that the nontrivial values of α in the TCP and in the CEP are consistent within the NJL model for both SU(2) and SU(3) versions of the model, and they reflect the effect of the TCP on the CEP. We also stress that the universality arguments are so general that they give no quantitative results and, due to the lack of information from the lattice simulations, they should be confronted with model calculations. Our results seem particularly interesting because the NJL model shares with QCD some features, such as the dynamics of chiral symmetry. In particular, the physics underlying the critical singularities in the QCD diagram is associated with this fundamental property of strong interaction. So, the NJL model is a useful framework allowing for insights to the difficult task of the analysis of the QCD phase diagram at finite temperature and chemical potential.

The eventual difference between the values of the C and χ_B critical exponents can be interesting in heavy-ion collision experiments.

VI. PARTIAL AND EFFECTIVE RESTORATION OF CHIRAL SYMMETRY

As we have shown in previous sections, thermodynamics provides a well-established procedure, as for instance the Gibbs criterion, to determine the critical points for the phase transition in the first order region. It follows that these critical points are signalized by the discontinuity of several relevant observables (masses, quark condensates) at some critical chemical potential, a situation that does not happen in the crossover region, where these observables are continuous. At present, the criterion most commonly accepted, and that will be used here, to define the critical point in the crossover region, is to identify this point as the inflection point of the quark masses $\partial^2 M/\partial T^2 = 0$ [23] or, equivalently, of the quark condensates [46,47]. This criterion is numerically equivalent to the one first proposed by M. Asakawa and K. Yazaki that defines the point where the constituent quark masses decrease to half of their values in the vacuum ($M_u = M_u(0)/2$) [48], as the critical point. From this point on the quark masses decrease quickly.

Both in the first order and in the crossover regions it is verified that the quark masses, especially for the nonstrange quarks, decrease strongly at the critical point. However, at this point different observables violating chiral

symmetry are still far from zero, like the quark condensates, the pion decay constant, and the difference between the masses of the chiral partners. One can say, therefore, that at the critical point there occurs only a *partial* restoration of chiral symmetry.

In view of what was said above we use the following criteria: we define the point in the $T - \mu_B$ plane for the phase transition associated with *partial* restoration of chiral symmetry as the inflexion (discontinuity) point for the quark masses, and define the point for *effective* restoration of chiral symmetry as that one where the masses of chiral partners become degenerate. This is also signaled by the merging of the π^0 and σ spectral functions [49].

As we include the strange sector in this study, the consequences of the nonvanishing anomaly term (mixing effects) on the strangeness content of mesons and mixing angles must be analyzed. In fact, as the temperature (density) increases, the mixing angles get close to their ideal values and the strangeness content of the mesons change [28,29]: the masses of the mesons that become almost nonstrange, σ and η, converge, respectively, with those of the nonstrange mesons π^0 and a_0, while that of the η', that becomes essentially strange, does not get close to f_0 (see [29] (Fig. 2, Case I)); the convergence of the chiral partner (κ, K), that has a $\bar{u}s$ structure, occurs at higher temperatures and is probably slowed by the small decrease of the constituent strange quark mass M_s. For the purpose of discussing the *effective* restoration of chiral symmetry, we restrict our analysis to the chiral partners (π^0, σ) that behave in a qualitatively similar manner as the pair (a_0, η).

The behavior of the masses of the chiral partners (π^0, σ) in the limiting cases $(T \neq 0, \rho_B = 0)$ and $(T = 0, \rho_B \neq 0)$ are qualitatively similar and well known from the literature: they both converge at a certain value of the temperature (density). The main difference between the finite temperature and the finite density case is that, in the first one, the degeneracy of the chiral partners occurs in a range of temperatures where the mesons are no longer bound states: the π^0 dissociates in $q\bar{q}$ pair at the Mott temperature $T_{M\pi^0} = 212$ MeV [22,27], and the σ at the Mott temperature $T_{M\sigma} = 160$ MeV; for the finite density case, the mesons are always bound states.

Interesting information can be obtained by calculating the masses of the π^0 and σ mesons as a function of T and $\rho_B(\mu_B)$ which allows us to obtain a curve in the $T - \rho_B(\mu_B)$ plane. This curve defines the line where the mesons became degenerate (Fig. 7). In Fig. 7 we also represent the "Mott lines" for the π^0 and the σ, as well as the critical line. As can be seen, the phase transition associated to *partial* restoration of chiral symmetry occurs above the Mott line for the pion and below the Mott line for the sigma, in most of the first order phase transition region; the opposite happens in the crossover region. Concerning the *effective* restoration of chiral symmetry, one can see, from the line of convergence of the chiral partners, that it happens after the *partial* restoration of chiral symmetry and the dissociation of the two mesons.

As we already saw, there are dramatic changes in the behavior of some thermodynamic functions such as the specific heat and the quark number susceptibilities around the CEP. So, due to their role as signals for restoration of chiral symmetry it is demanding to discuss the behavior of the chiral partners (π^0, σ).

First we notice, in Fig. 7, that the two Mott lines cross in the first order region at a point just bellow the CEP. This is probably a remnant of the situation in the chiral limit where the transition is second order and the pion and sigma dissociate at the same point.

In Fig. 8 we plot the pion and sigma masses as functions of the baryonic chemical potential for three different temperatures: $T = 40$ MeV $< T^{\mathrm{CEP}}$, $T^{\mathrm{CEP}} = 67.7$ MeV, and $T = 100$ MeV $> T^{\mathrm{CEP}}$. For $T = 40$ MeV and $\mu_B \approx 350$ MeV, a discontinuity is visible in the evolution of the masses, signaling a first order phase transition. However, according to our criterion, the *effective* restoration of the chiral symmetry only happens at $\mu_B \approx 380$ MeV. At the CEP ($T = 67.7$ MeV; $\mu_B = 318.4$ MeV), the sharp decrease (increase) of the sigma

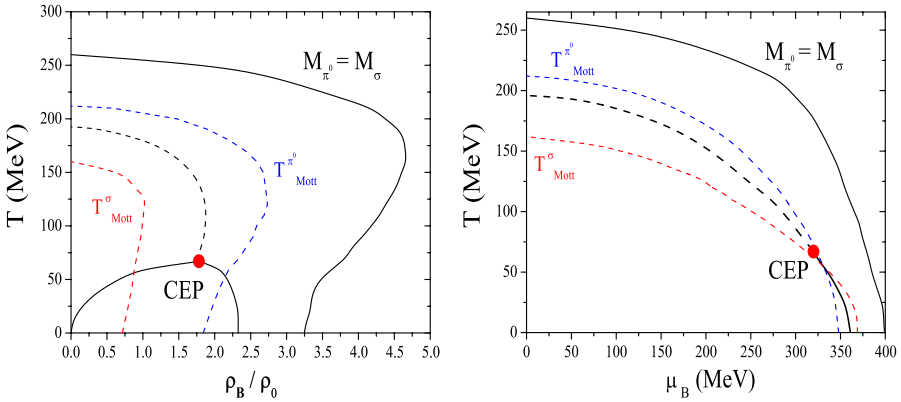

FIG. 7 (color online). The *effective* restoration of chiral symmetry, the phase transition, and the Mott lines for π^0 and σ mesons in the $T - \rho_B(\mu_B)$ plane.

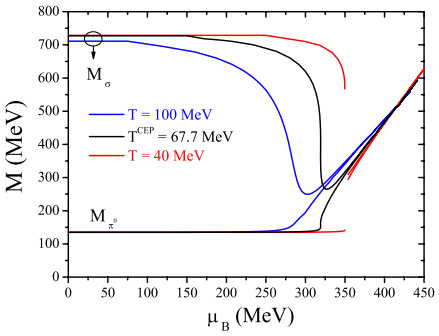

FIG. 8 (color online). Degeneracy of the chiral partners (π^0, σ) for different temperatures around the CEP.

(pion) meson masses reflect the nature of the second order phase transition. Once again the *effective* restoration of chiral symmetry only happens at $\mu_B \approx 370$ MeV. When $T = 100$ MeV $> T^{\mathrm{CEP}}$, we have a crossover and the meson masses have a smooth behavior. In this case, the *effective* restoration of the chiral symmetry happens at $\mu_B \approx 355$ MeV.

VII. CONCLUSIONS

The properties of the QCD transition at vanishing chemical potential depend on the number of quark flavors and on their masses. The critical temperatures of $T_c \approx 155$ MeV or as high as $T_c \approx 260$ MeV have been reported in the literature. Presently, considering also nonvanishing chemical potential, some lattice calculations locate the CEP at $T \approx 160$ MeV and $\mu_B \approx 360$ MeV [6]. However, the existence and location of the CEP are not conclusive even for lattice calculations [50].

We proved that our model calculation has been able to reproduce the qualitative phase structure features, and we also obtain the location of the CEP. We have obtained, at zero baryon chemical potential in the SU(3) NJL model, values for the critical temperature around 120–200 MeV. The transition is first order in the chiral limit ($m_u = m_d = m_s = 0$). Furthermore, when $m_u = m_d = 0$ and $m_s > m_s^{\mathrm{crit}}$ ($m_s^{\mathrm{crit}} = 18.3$ MeV) the transition is of second order ending in a first order line at the TCP. Finally, when also $m_u = m_d \neq 0$, there is a crossover for all values of m_s and the location of the CEP depends strongly on the strange quark mass. Contrarily to what happens in the three-flavor NJL model, we find a TCP in the two-flavor NJL model in the chiral limit. This agrees with what is expected at $\mu_B = 0$: for $m_i = 0$ the chiral restoration happens via a second order phase transition for $N_f = 2$, and via a first order for $N_f \geq 3$. For realistic values of the current quark masses the CEP is located at $T^{\mathrm{CEP}} = 79.9$ MeV and $\mu_B^{\mathrm{CEP}} = 331.7$ MeV for $N_f = 2$, and at $T^{\mathrm{CEP}} = 67.7$ MeV and $\mu_B^{\mathrm{CEP}} = 318.4$ MeV for $N_f = 3$.

The pattern characteristic of a first order phase transition has also been analyzed through several equations of state and the latent heat. For example, we verified that states (droplets) in mechanical equilibrium with the vacuum state at $P = 0$ are found at zero temperature. This leads to nontrivial consequences for the behavior of the isentropic trajectories which terminate at $T = 0$ at the first order transition line. Our convenient choice of the model parameters, which allows for a first order phase transition that is stronger than in other treatments of the NJL model, is crucial to attain this result.

We have studied the baryon number susceptibility and the specific heat which are related with event-by-event fluctuations of μ_B or T in heavy-ion collisions. In the two and three-flavor NJL models, for χ_B, we conclude that the obtained critical exponents around the CEP in both models are consistent with the mean field values $\epsilon = \epsilon' = 2/3$. For the specific heat we obtain nontrivial exponents $1/2 < \alpha < 2/3$ around the CEP, indicating a crossover of different universality classes [13,44]. This effect is more clearly visible for the critical exponent of the specific heat in the SU(2) version of the NJL model, where a crossover from α to α_1 is also observed. Nevertheless we notice that the values of α in the TCP and in the CEP are consistent within both versions of the NJL model. A better insight to the difficult task of the analysis of the phase diagram of QCD can be provided by an extension of the NJL model where quarks interact with the temporal gluon field represented by the Polyakov loop dynamics [4,43,49,51]. Work in this direction is in progress.

Concerning the behavior of the chiral partners in the vicinity of the CEP, we verified that the two Mott lines, respectively, for σ and π^0 cross at a point just below the CEP. On the other hand, there is a sharp decrease (increase) of the sigma (pion) meson masses at the CEP, which reflects the nature of the second order phase transition at this point.

ACKNOWLEDGMENTS

Work supported by Grant No. SFRH/BPD/23252/2005 (P. Costa), Centro de Física Teórica, FCT under Project No. POCI/FP/63945/2005 and under Project No. PTDC/FP/63912/2005 (GTAE).

APPENDIX

In this appendix we give the integrals appearing in the meson propagators, in the vacuum, and at finite temperature and density, as well as some useful expressions concerning the σ meson.

The integrals I_1^i and $I_2^{ij}(P_0)$ are given by

$$I_1^i(T, \mu_i) = \frac{N_c}{4\pi^2} \int \frac{\mathrm{p}^2 d\mathrm{p}}{E_i} (1 - n_i - \bar{n}_i), \tag{A1}$$

$$I_2^{ii}(P_0, T, \mu_i) = \frac{N_c}{2\pi^2} \mathcal{P} \int \frac{\mathrm{p}^2 d\mathrm{p}}{E_i} \frac{1}{4E_i^2 - P_0^2} (1 - n_i - \bar{n}_i), \tag{A2}$$

where $E_i = \sqrt{\mathrm{p}^2 + M_i^2}$ is the quark energy. To regularize the integrals we introduce the 3-dimensional cutoff parameter Λ. When $P_0 > 2M_i$ it is necessary to take into account the imaginary part of the second integral. It may be found, with help of the $i\epsilon$ -prescription $P_0^2 \to P_0^2 - i\epsilon$. Using

$$\lim_{\epsilon \to 0^+} \frac{1}{y - i\epsilon} = \mathcal{P}\frac{1}{y} + i\pi\delta(y) \tag{A3}$$

we obtain the integral

$$I_2^{ii}(P_0, T, \mu_i) = \frac{N_c}{2\pi^2}\mathcal{P}\int \frac{\mathrm{p}^2 d\mathrm{p}}{E_i}\frac{1}{4E_i^2 - P_0^2}(1 - n_i - \bar{n}_i) + i\frac{N_c}{16\pi}\sqrt{1 - \frac{4M_i^2}{P_0^2}}\Big[1 - n_i\Big(\frac{P_0}{2}\Big) - \bar{n}_i\Big(\frac{P_0}{2}\Big)\Big]. \tag{A4}$$

Concerning the calculation of the propagator for the σ meson, the projector S_{ab} and the polarization operator Π_{ab}^S matrices, in the case $\langle\bar{q}_u q_u\rangle = \langle\bar{q}_d q_d\rangle$, have the nonvanishing elements

$$S_{33} = g_S - g_D\langle\bar{q}_s q_s\rangle, \tag{A5}$$

$$S_{00} = g_S + \tfrac{2}{3}g_D(\langle\bar{q}_u q_u\rangle + \langle\bar{q}_d q_d\rangle + \langle\bar{q}_s q_s\rangle), \tag{A6}$$

$$S_{88} = g_S - \tfrac{1}{3}g_D(2\langle\bar{q}_u q_u\rangle + 2\langle\bar{q}_d q_d\rangle - \langle\bar{q}_s q_s\rangle), \tag{A7}$$

$$S_{08} = S_{80} = -\tfrac{1}{3\sqrt{2}}g_D(\langle\bar{q}_u q_u\rangle + \langle\bar{q}_d q_d\rangle - 2\langle\bar{q}_s q_s\rangle). \tag{A8}$$

Analogously, we get

$$\Pi_{00}^S(P_0) = \tfrac{2}{3}[J_{uu}^S(P_0) + J_{dd}^S(P_0) + J_{ss}^S(P_0)], \tag{A9}$$

$$\Pi_{88}^S(P_0) = \tfrac{1}{3}[J_{uu}^S(P_0) + J_{dd}^S(P_0) + 4J_{ss}^S(P_0)], \tag{A10}$$

$$\Pi_{08}^S(P_0) = \Pi_{80}^S(P_0) = \tfrac{\sqrt{2}}{3}[J_{uu}^S(P_0) + J_{dd}^S(P_0) - 2J_{ss}^S(P_0)], \tag{A11}$$

where

$$J_{ii}^S(P_0) = 4[2I_1^i + [P_0^2 - 4M_i^2]I_2^{ii}(P_0)]. \tag{A12}$$

[1] M. Alford, K. Rajagopal, and F. Wilczek, Phys. Lett. B **422**, 247 (1998); Nucl. Phys. **B537**, 443 (1999).
[2] R. Rapp, T. Schäfer, E. V. Shuryak, and M. Velkovsky, Phys. Rev. Lett. **81**, 53 (1998).
[3] M. A. Halasz, A. D. Jackson, R. E. Shrock, M. A. Stephanov, and J. J. M. Verbaarschot, Phys. Rev. D **58**, 096007 (1998).
[4] C. Ratti, M. A. Thaler, and W. Weise, Phys. Rev. D **73**, 014019 (2006).
[5] J. Liao and E. Shuryak, Nucl. Phys. **A775**, 224 (2006).
[6] Z. Fodor and S. D. Katz, J. High Energy Phys. 04 (2004) 050.
[7] F. Wilczek, Int. J. Mod. Phys. A **7**, 3911 (1992).
[8] K. Rajagopal and F. Wilczek, Nucl. Phys. **B399**, 395 (1993).
[9] A. Ukawa, Nucl. Phys. B, Proc. Suppl. **53**, 106 (1997).
[10] M. Buballa and M. Oertel, Nucl. Phys. **A642**, c39 (1998).
[11] M. Buballa and M. Oertel, Phys. Lett. B **457**, 261 (1999).
[12] M. Stephanov, K. Rajagopal, and E. Shuryak, Phys. Rev. Lett. **81**, 4816 (1998).
[13] Y. Hatta and T. Ikeda, Phys. Rev. D **67**, 014028 (2003).
[14] T. M. Schwarz, S. P. Klevansky, and G. Papp, Phys. Rev. C **60**, 055205 (1999).
[15] P. Costa, C. A. de Sousa, M. C. Ruivo, and Yu. L. Kalinovsky, Phys. Lett. B **647**, 431 (2007).
[16] H. Appelshauser and H. Sako (CERES Collaboration), Nucl. Phys. **A752**, 394 (2005); J. T. Mitchell (PHENIX Collaboration), J. Phys. Conf. Ser. **27**, 88 (2005).
[17] L. Stodolsky, Phys. Rev. Lett. **75**, 1044 (1995).
[18] R. Korus *et al.*, Phys. Rev. C **64**, 054908 (2001).
[19] A. Barducci *et al.*, Phys. Lett. B **231**, 463 (1989); Phys. Rev. D **41**, 1610 (1990); **49**, 426 (1994).
[20] Y. Nambu and G. Jona-Lasinio, Phys. Rev. **122**, 345 (1961); **124**, 246 (1961).
[21] T. Hatsuda and T. Kunihiro, Phys. Rep. **247**, 221 (1994).
[22] P. Rehberg, S. P. Klevansky, and J. Hüfner, Phys. Rev. C **53**, 410 (1996).
[23] M. Buballa, Phys. Rep. **407**, 205 (2005).
[24] L. D. McLerran, Phys. Rev. D **36**, 3291 (1987).
[25] M. Asakawa, U. Heinz, and B. Müller, Phys. Rev. Lett. **85**, 2072 (2000).
[26] J. P. Blaizot, E. Iancu, and A. Rebhan, Phys. Lett. B **523**, 143 (2001).
[27] P. Costa, M. C. Ruivo, C. A. de Sousa, and Y. L. Kalinovsky, Phys. Rev. C **70**, 025204 (2004).
[28] P. Costa, M. C. Ruivo, C. A. de Sousa, and Y. L. Kalinovsky, Phys. Rev. D **70**, 116013 (2004); P. Costa, M. C. Ruivo, and Yu. L. Kalinovsky, Phys. Lett. B **560**, 171 (2003); **577**, 129 (2003).
[29] P. Costa, M. C. Ruivo, C. A. de Sousa, and Y. L. Kalinovsky, Phys. Rev. D **71**, 116002 (2005).
[30] I. N. Mishustin, L. M. Satarov, H. Stöcker, and W. Greiner, Phys. Rev. C **62**, 034901 (2000).
[31] K. Rajagopal, Nucl. Phys. **A661**, 150 (1999); J. Berges and K. Rajagopal, Nucl. Phys. **B538**, 215 (1999).
[32] O. Scavenius, A. Mocsy, I. N. Mishusti, and D. H. Rischke, Phys. Rev. C **64**, 045202 (2001).
[33] S. Ejiri, F. Karsch, E. Laermann, and C. Schmidt, Phys. Rev. D **73**, 054506 (2006).
[34] M. Stephanov, K. Rajagopal, and E. Shuryak, Phys. Rev. D **60**, 114028 (1999).
[35] C. Nonaka and M. Asakawa, Phys. Rev. C **71**, 044904

(2005).
[36] P. Zhuang, J. Hufner, and S. P. Klevansky, Nucl. Phys. **A576**, 525 (1994).
[37] P. Costa, M. C. Ruivo, and C. A. de Sousa, arXiv:0710.5491.
[38] P. R. Subramanian, H. Stocker, and W. Greiner, Phys. Lett. B **173**, 468 (1986).
[39] E. Laermann and O. Philipsen, Annu. Rev. Nucl. Part. Sci. **53**, 163 (2003).
[40] S. D. H. Hsu and M. Schwetz, Phys. Lett. B **432**, 203 (1998).
[41] A. Barducci, R. Casalbuoni, G. Pettini, and L. Ravagli, Phys. Rev. D **72**, 056002 (2005).
[42] R. D. Pisarski and F. Wilczek, Phys. Rev. D **29**, 338 (1984).
[43] C. Sasaki, B. Friman, and K. Redlich, Phys. Rev. D **75**, 054026 (2007); **75**, 074013 (2007).
[44] B.-J. Schaefer and J. Wambach, Phys. Rev. D **75**, 085015 (2007).
[45] R. B. Griffiths and J. Wheeler, Phys. Rev. A **2**, 1047 (1970).
[46] B. Allés, M. D'Elia, and A. Giacomo, Nucl. Phys. **B494**, 281 (1997).
[47] M. C. Ruivo, P. Costa, C. A. de Sousa, and Yu. L. Kalinovsky, J. Phys. G **31**, S1183 (2005).
[48] M. Asakawa and K. Yazaki, Nucl. Phys. **A504**, 668 (1989).
[49] H. Hansen, W. M. Alberico, A. Beraudo, A. Molinari, M. Nardi, and C. Ratti, Phys. Rev. D **75**, 065004 (2007).
[50] P. de Forcrand and O. Philipsen, J. High Energy Phys. 01 (2007) 077; Nucl. Phys. **B673**, 170 (2003); **B642**, 290 (2002); O. Philipsen, arXiv:0710.1217.
[51] E. Megias, E. Ruiz Arriola, and L. L. Salcedo, Phys. Rev. D **74**, 065005 (2006); **74**, 114014 (2006).